

# High-precision determination of the electric and magnetic radius of the proton

Yong-Hui Lin<sup>a</sup>, Hans-Werner Hammer<sup>b,c</sup>, Ulf-G. Meißner<sup>a,d,e</sup>

<sup>a</sup>*Helmholtz-Institut für Strahlen- und Kernphysik and Bethe Center for Theoretical Physics, Universität Bonn, D-53115 Bonn, Germany*

<sup>b</sup>*Technische Universität Darmstadt, Department of Physics, Institut für Kernphysik, 64289 Darmstadt, Germany*

<sup>c</sup>*ExtreMe Matter Institute EMMI, GSI Helmholtzzentrum für Schwerionenforschung GmbH, 64291 Darmstadt, Germany*

<sup>d</sup>*Institute for Advanced Simulation, Institut für Kernphysik and Jülich Center for Hadron Physics, Forschungszentrum Jülich, D-52425 Jülich, Germany*

<sup>e</sup>*Tbilisi State University, 0186 Tbilisi, Georgia*

---

## Abstract

Using dispersion theory with an improved description of the two-pion continuum based on the precise Roy-Steiner analysis of pion-nucleon scattering, we analyze recent data from electron-proton scattering. This allows for a high-precision determination of the electric and magnetic radius of the proton,  $r_E = (0.838^{+0.005+0.004}_{-0.004-0.003})$  fm and  $r_M = (0.847 \pm 0.004 \pm 0.004)$  fm, where the first error refers to the fitting procedure using bootstrap and the data while the second one refers to the systematic uncertainty related to the underlying spectral functions.

---

## 1. Introduction

The electric radius,  $r_E$ , and the magnetic radius,  $r_M$ , of the proton are fundamental quantities of low-energy QCD, as they are a measure of the probe-dependent size of the proton. While the electric radius of the proton has attracted much attention in the last decade (see, e.g., Refs. [1, 2, 3] for recent reviews), this is not true for its magnetic counterpart, which is not probed in the Lamb shift in electronic or muonic hydrogen. A major source of information on the proton form factors (and the corresponding radii) is elastic electron-proton ( $ep$ ) scattering. These data can be best analyzed in the time-honored framework of dispersion theory [4, 5, 6, 7], which includes all constraints from unitarity, analyticity and crossing symmetry and is consistent with the strictures from perturbative QCD at very large momentum transfer [8]. Of particular importance for the proper extraction of the radii is the isovector two-pion continuum on the left shoulder of the  $\rho$ -resonance [9, 10], which can be worked out model-independently using dispersively constructed pion-nucleon scattering amplitudes combined with data of the pion vector form factor. Based on the recent Roy-Steiner analysis of pion-nucleon scattering [11], an improved determination of the two-pion continuum was given in Ref. [12], which also includes thorough error estimates. Using a sum rule for the isovector charge radius, in that paper a squared isovector charge radius,  $(r_E^v)^2 = 0.405(36)$  fm<sup>2</sup>, was obtained which is in perfect agreement with a recent state-of-the-art lattice QCD calculation at physical pion masses,  $(r_E^v)^2 = 0.400(13)_{\text{sta}}(11)_{\text{sys}}$  fm<sup>2</sup> [13]. This underscores the importance of the isovector two-pion continuum for the form factors and demonstrates the consistency of the new and improved representation from Ref. [12] with QCD. This new representation of the two-pion continuum has so far not been employed in any dispersion-theoretical analysis of form factor data.

With the advent of new and precise electron-scattering data at low momentum transfer from Jefferson Laboratory (PRad collaboration) [14], it is timely to analyze these together with the precise data from the A1 collaboration at the Mainz Microtron (MAMI) [15] using the improved two-pion continuum contribution. Given the precision of these data and of the underlying formalism, this will allow for a high-precision determination of both the electric and the magnetic form factors and the corresponding

radii,  $r_E$  and  $r_M$ , respectively. Clearly, this is an important step in pinning down these fundamental quantities with high precision. Other recent analyses of the PRad and Mainz data can be found in Refs. [16, 17, 18] and will be discussed below.

## 2. Formalism

Here, we briefly summarize the underlying formalism, which is detailed in Refs. [19, 20]. The differential cross section for  $ep$  scattering can be expressed through the electric ( $G_E$ ) and magnetic ( $G_M$ ) Sachs form factors (FFs) as

$$\frac{d\sigma}{d\Omega} = \left( \frac{d\sigma}{d\Omega} \right)_{\text{Mott}} \frac{\tau}{\epsilon(1+\tau)} \left[ G_M^2(t) + \frac{\epsilon}{\tau} G_E^2(t) \right], \quad (1)$$

where  $\epsilon = [1 + 2(1 + \tau) \tan^2(\theta/2)]^{-1}$  is the virtual photon polarization,  $\theta$  is the electron scattering angle in the laboratory frame,  $\tau = -t/4m_N^2$ , with  $t$  the four-momentum transfer squared and  $m_N$  the nucleon mass. Moreover,  $(d\sigma/d\Omega)_{\text{Mott}}$  is the Mott cross section, which corresponds to scattering off a point-like spin-1/2 particle. Since  $-t \equiv Q^2 > 0$  is spacelike in  $ep$  scattering, the form factors are often displayed as a function of  $Q^2$ . Equation (1) will be our basic tool to analyze the data together with the two-photon corrections from Ref. [20].

The electric and magnetic radii of the proton, which are at the center of this investigation, are given by

$$r_{E/M} = \left( \frac{6}{G_{E/M}(0)} \frac{dG_{E/M}(t)}{dt} \Big|_{t=0} \right)^{1/2}. \quad (2)$$

For the theoretical analysis, it is advantageous to use the Dirac ( $F_1$ ) and Pauli ( $F_2$ ) FFs, which are linear combinations of the Sachs FFs:

$$G_E(t) = F_1(t) - \tau F_2(t), \quad G_M(t) = F_1(t) + F_2(t). \quad (3)$$

The FFs for spacelike momentum transfer,  $t < 0$ , are given in terms of an unsubtracted dispersion relation,

$$F_i(t) = \frac{1}{\pi} \int_{t_0}^{\infty} \frac{\text{Im}F_i(t') dt'}{t' - t}, \quad i = 1, 2, \quad (4)$$

with  $t_0 = 4M_\pi^2 (9M_\pi^2)$  the isovector (isoscalar) threshold, and  $M_\pi$  is the charged pion mass. The spectral functions are expressed in terms of (effective) vector meson poles and continua, which leads to the following representation of the FFs:

$$\begin{aligned} F_i^s(t) &= \sum_{V=\omega, \phi, s_1, s_2, \dots} \frac{a_i^V}{m_V^2 - t} + F_i^{\pi\rho}(t) + F_i^{\bar{K}K}(t), \\ F_i^v(t) &= \sum_{V=v_1, v_2, \dots} \frac{a_i^V}{m_V^2 - t} + F_i^{2\pi}(t), \end{aligned} \quad (5)$$

with  $i = 1, 2$ , in terms of the isoscalar ( $s$ ) and isovector ( $v$ ) components,  $F_i^{(s/v)} = (F_i^p \pm F_i^n)/2$ . This representation is advantageous for dispersion analyses since the intermediate states contributing to the spectral function have good isospin. In the isoscalar spectral function, the first two poles correspond to the  $\omega(782)$  and the  $\phi(1020)$  mesons, so these masses are fixed and the residues are bounded as in Ref. [20]. Furthermore, we take into account the  $\pi\rho$  and  $\bar{K}K$  continua as explained in detail in Ref. [19]. The last term in the isovector form factor corresponds to the parameterization of the two-pion continuum taken from Ref. [11]. This is the essential new theory input compared to earlier dispersive analyses. The higher mass poles are effective poles that parameterize the spectral function at large  $t$ . We explicitly check in our analysis that the radii are insensitive to the details of this parameterization. The fit parameters are therefore the various vector meson residues  $a_i^V$  and the masses of the additional vector mesons  $s_i, v_i$ .

Note that from the proton data alone, the isospin of a given pole is not determined. We simply assign a given number of isoscalar and isovector poles besides the continuum contributions, which have a given isospin, as well as the  $\omega$  and  $\phi$  mesons (see also the discussion in the Appendix). In addition, we fulfill the normalization conditions  $F_1(0) = 1$  (in units of the elementary charge  $e$ ) and  $F_2(0) = \mu_p$ , with  $\mu_p$  the anomalous magnetic moment of the proton. To ensure the stability of the fit [21], we demand that the residua of the vector meson poles are bounded,  $|a_i^V| < 5 \text{ GeV}^2$ , and that no effective poles with masses below 1 GeV appear. Finally, the FFs must satisfy the superconvergence relations

$$\int_{t_0}^{\infty} \text{Im}F_i(t)t^n dt = 0, \quad i = 1, 2, \quad (6)$$

with  $n = 0$  for  $F_1$  and  $n = 0, 1$  for  $F_2$ , corresponding to the fall-off with inverse powers of  $Q^2$  at large momentum transfer as demanded by perturbative QCD [8].

These parameterizations (5) are used in Eq. (1) and the number of isoscalar and isovector poles is determined by the condition to obtain the best fit to the data. The quality of the fits is measured in terms of the traditional  $\chi^2$ ,

$$\chi_1^2 = \sum_i \sum_k \frac{(n_k C_i - C(Q_i^2, \theta_i, \vec{p}))^2}{(\sigma_i + \nu_i)^2}, \quad (7)$$

where  $C_i$  are the cross section data at the points  $Q_i^2, \theta_i$  and  $C(Q_i^2, \theta_i, \vec{p})$  are the cross sections for a given FF parameterization for the parameter values contained in  $\vec{p}$ . Moreover,  $n_k$  are normalization coefficients for the various data sets (labelled by the integer  $k$ ), while  $\sigma_i$  and  $\nu_i$  are their statistical and systematical errors, respectively. A more refined definition of the  $\chi^2$  is given by [20]

$$\chi_2^2 = \sum_{i,j} \sum_k (n_k C_i - C(Q_i^2, \theta_i, \vec{p})) [V^{-1}]_{ij} (n_k C_j - C(Q_j^2, \theta_j, \vec{p})), \quad (8)$$

in terms of the covariance matrix  $V_{ij} = \sigma_i \sigma_j \delta_{ij} + \nu_i \nu_j$ . Theoretical errors will be calculated on the one hand using a bootstrap method. We simulate a large number of data sets by randomly varying the points in the original set within the given errors assuming their normal distribution. We then fit to each of them separately, derive the radius from each fit, and analyze the distribution of these radius values (see App. D of Ref. [20] for details). On the other hand theoretical errors are estimated by varying the number of effective vector meson poles. The first error thus gives the uncertainty due to the fitting procedure (bootstrap) and the data while the second one reflects the accuracy of the spectral functions underlying the dispersion-theoretical analysis. Note that these two errors are not in a strict one-to-one correspondence to the commonly given statistical and systematic errors. We further remark that since the effect of the two-photon corrections on the extracted radii is minimal, we do not attempt to quantify their uncertainty here (see also the discussion in [22] and references therein).

### 3. Results

As a first validation of our method, we only consider the PRad data [14]. These can be best fitted with the lowest two isoscalar mesons (the  $\omega$  and the  $\phi$ ) and two additional isovector ones ( $2s + 2v$  poles). Fitting with statistical errors only (as in Ref. [14]), we have a  $\chi^2/\text{dof} = 1.33$ , completely consistent with the results reported there. Including also the systematic errors, the reduced  $\chi^2$  is slightly improved and we find as central values

$$r_E = (0.829 \pm 0.012 \pm 0.001) \text{ fm}, \quad r_M = (0.843 \pm 0.007_{-0.012}^{+0.018}) \text{ fm}, \quad (9)$$

consistent with the PRad result,  $r_E = (0.831 \pm 0.007_{\text{stat}} \pm 0.012_{\text{syst}}) \text{ fm}$  for the electric radius. In our case, the first error is obtained by bootstrap using 1000 samples and the second error is obtained by varying the number of poles from two isoscalar and two isovector ones (which gives the best solution) up to 5 isoscalar plus 5 isovector poles. While the absolute  $\chi^2$  of these 8 different solutions is almost the same,

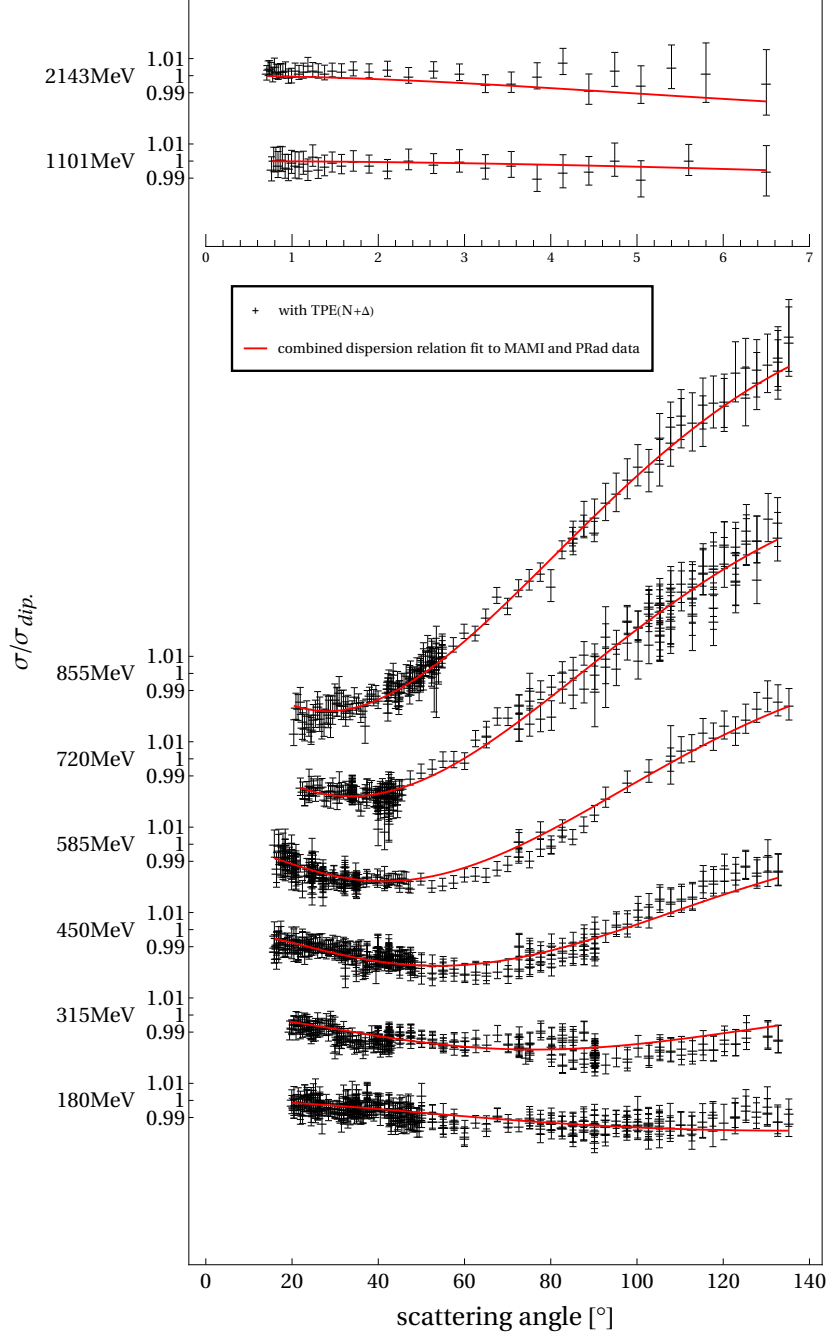


Figure 1: Combined fit to the PRad (upper panel) and the Mainz data (lower panel) as described in the text. The dipole cross section  $\sigma_{dip}$  is obtained by using the dipole approximation to the FFs.

the  $\chi^2/\text{dof}$  increase from 1.33 to 1.61. Note also that the uncertainty in the magnetic radius is sizeably larger than the one of the electric radius, which is due to the fact that at the very low  $Q^2$  probed by PRad, the electric form factor dominates the cross section. We remark that the PRad data have also been analyzed in Ref. [23] using the  $z$ -expansion, which also finds a sizeably increased statistical error as done here.

Next, we turn to the combined analysis of the Mainz and the PRad data. We note that we increase the

	This work	Ref. [16]	Ref. [17]	Ref. [18]
$r_E$ [fm]	$0.838^{+0.005+0.004}_{-0.004-0.003}$	$0.842 \pm 0.002_{\text{fit}} \pm 0.010_{\text{th}}$	$0.847 \pm 0.008_{\text{sta}}$	$0.852 \pm 0.002_{\text{sta}} \pm 0.009_{\text{sys}}$
$r_M$ [fm]	$0.847 \pm 0.004 \pm 0.004$	$0.850 \pm 0.001_{\text{fit}} \pm 0.010_{\text{th}}$	—	—

Table 1: Comparison of the proton radii extracted in this work and other recent papers. For the definitions of the errors in Refs. [16, 17, 18], see these papers.

weight of the PRad data by a factor ten in the combined  $\chi^2$ . This is legitimate as the PRad data probe much smaller momentum transfer than the Mainz data and thus should be enhanced. Changing this weight by a factor of two leads to changes in the proton radii that are well covered by the uncertainties discussed below. The best fit to these data is shown in Fig. 1 for the PRad data and the Mainz data (normalized to the dipole cross section  $\sigma_{\text{dip}}$ ). To best describe these combined data sets requires  $5s + 5v$  poles (as in Ref. [20] for the MAMI data alone) with a  $\chi^2/\text{dof} = 1.25$ . The corresponding vector meson parameters (masses, residua) and the normalization constants of the various data sets are collected and discussed in Appendix A. In such a combined fit, the PRad data are described slightly worse than before, as the Mainz data set is much larger and has also smaller error bars. The resulting radii are:

$$\begin{aligned}
r_E &= (0.838^{+0.005+0.004}_{-0.004-0.003}) \text{ fm} , \\
r_M &= (0.847 \pm 0.004 \pm 0.004) \text{ fm} .
\end{aligned}
\tag{10}$$

These results are consistent with our earlier dispersion-theoretical determinations [22, 20] but have much improved and smaller uncertainties. In particular, the fit error based on bootstrap (using 5000 samples) is considerably improved as compared to Ref. [20] which is related to the new PRad data, while the fit error for the magnetic radius is similar (as it is dominated by the Mainz data). The theory error estimate is obtained performing 11 different sets of fits with varying numbers of isoscalar and isovector poles, from  $2s + 2v$  to  $7s + 7v$  poles, where the reduced  $\chi^2/\text{dof}$  only varies by less than 3% from the optimal value obtained for  $5s + 5v$  poles. Note further that the theory uncertainty is improved compared to the one in Ref. [22], with the differences that we do not include neutron data here and a much better and precise determination of the so important isovector two-pion continuum is employed.

In Table 1 we have collected these results together with other recent determinations of  $r_E$  and  $r_M$  employing both the PRad and the Mainz data. Within the quoted errors all extracted radii are consistent. The analysis in Ref. [16] is similar to ours. In contrast to our approach, however, it employs a dispersively improved chiral perturbation theory representation of the two-pion continuum. This approach is subject to uncertainties in the  $\rho$ -region as stressed in Ref. [24], different from the exact representation used here. The work of Ref. [17] can not be directly compared, as it is based on a continued fraction approach which has no relation to the dispersion-theoretical method used here. Also, in that paper no value for the magnetic radius is given. Similar remarks hold for the work of Ref. [18], which applies various fit functions (not guided by unitarity) to the flavor-dependent Dirac form factors with  $Q^2 \leq 1 \text{ GeV}^2$  to extract the proton and the neutron charge radii. We note that our charge radius is also consistent with the current CODATA value,  $r_E = 0.8414(19) \text{ fm}$  [25]. Moreover, it is in agreement with the value  $r_E = 0.827(20) \text{ fm}$  obtained by combining the recent precise lattice result by Djukanovic et al. for the isovector radius with the experimental neutron charge radius [13, 26]. Another recent lattice study calculated the proton charge radius directly but neglected disconnected contributions to the isoscalar current, which are computationally very expensive [27]. Because of this, the charge radius comes out smaller but their isovector result is in agreement with Ref. [13] and the experimental value.<sup>1</sup> Thus finally a consistent picture for the proton charge radius appears to emerge [2].

In Fig. 2 (left panel), we show the resulting electric and magnetic FF of the proton normalized to the

---

<sup>1</sup>For a detailed discussion of previous lattice QCD calculations we refer to Refs. [13, 27].

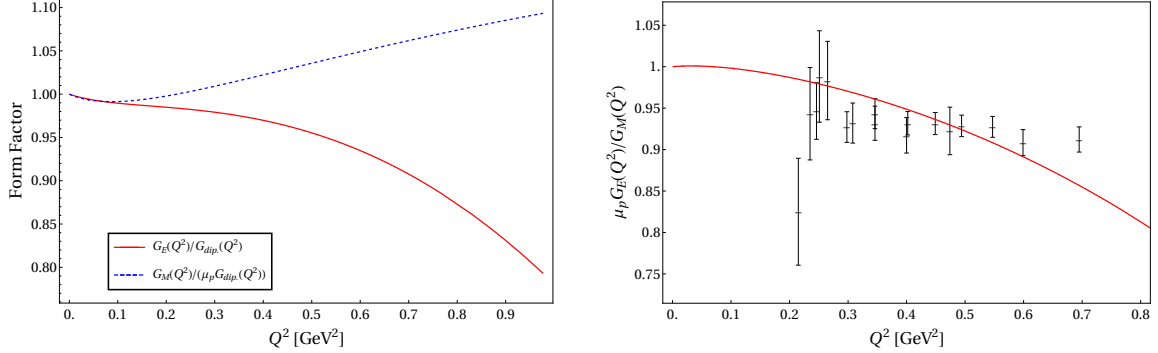


Figure 2: Left panel: Electric (red solid line) and magnetic (blue dashed line) FF normalized to the dipole FF for our best solution,  $G_E(Q^2)/G_{\text{dip}}(Q^2)$  and  $G_M(Q^2)/(\mu_p G_{\text{dip}}(Q^2))$ , respectively. Right panel: FF ratio  $\mu_p G_E(Q^2)/G_M(Q^2)$  (red solid line) compared to the data of Refs. [28, 29].

dipole FF,  $G_{\text{dip}}(Q^2) = (1 + Q^2/Q_{\text{dip}}^2)^{-2}$ , with  $Q_{\text{dip}}^2 = 0.71 \text{ GeV}^2$ . These show a behavior similar to what was found in earlier dispersion-theoretical studies, and we note that again physically constrained fits do not produce oscillations as seen, e.g., the the magnetic form factor in Ref. [15]. We refrain here from displaying the corresponding uncertainty estimates to avoid clutter. In the right panel of Fig. 2, the FF ratio  $\mu_p G_E(Q^2)/G_M(Q^2)$  is displayed together with the data of Refs. [28, 29]. Our ratio is consistent with these data, which were not included in the fits.

#### 4. Summary

In this paper, we have continued the dispersion-theoretical analysis of the proton form factors triggered by two main developments. On the theoretical side, a much improved representation of the two-pion-continuum contribution to the isovector spectral function based on the precision results from the Roy-Steiner analysis of pion-nucleon scattering has been presented [11]. On the experimental side, new  $ep$  scattering data at very low  $Q^2$  from the PRad collaboration [14] have become available. Using our improved spectral functions and employing the two-photon corrections worked out in Ref. [20], we have analyzed these new data as well as the combination of the PRad and the Mainz data [15] which allowed us to extract the proton's electric and magnetic radius with unprecedented precision, as given in Eq. (10). Theoretical uncertainties from the fit procedure and from variations in the spectral functions have been worked out. In the future, Bayesian methods will be used to further improve these uncertainty estimates. Furthermore, fits including also the time-like proton form factor data should be performed. Finally, data for the scattering off the neutron should be included, as these can be used to precisely pin down the corresponding neutron radii using chiral effective field theory for few-nucleon systems [26].

#### Acknowledgements

This work of UGM and YHL is supported in part by the NSFC and the Deutsche Forschungsgemeinschaft (DFG, German Research Foundation) through the funds provided to the Sino-German Collaborative Research Center TRR110 ‘‘Symmetries and the Emergence of Structure in QCD’’ (NSFC Grant No. 12070131001, DFG Project-ID 196253076 - TRR 110), by the Chinese Academy of Sciences (CAS) through a President’s International Fellowship Initiative (PIFI) (Grant No. 2018DM0034), by the VolkswagenStiftung (Grant No. 93562), and by the EU Horizon 2020 research and innovation programme, STRONG-2020 project under grant agreement No. 824093. HWH was supported by the Deutsche Forschungsgemeinschaft (DFG, German Research Foundation) – Projektnummer 279384907 – CRC 1245 and by the German Federal Ministry of Education and Research (BMBF) (Grant No. 05P18RDFN1).

## Appendix A. Fit parameters and discussion

We collect the various vector meson masses and couplings that appear in the spectral functions Eqs. (5) and the normalization constants of the various data sets (see Ref. [20] for precise definitions) in Table A.2.

$V_s$	$m_V$	$a_1^V$	$a_2^V$	$V_v$	$m_V$	$a_1^V$	$a_2^V$
$\omega$	0.7830	0.8572	0.0177	$v_1$	1.0426	0.6876	-1.5086
$\phi$	1.0190	-1.3155	0.9955	$v_2$	2.3839	-4.3848	4.8535
$s_1$	1.4790	2.6928	-4.8054	$v_3$	3.3482	-3.6869	-4.6070
$s_2$	2.2381	1.6155	4.8620	$v_4$	3.5665	2.4907	-3.0026
$s_3$	3.4614	-2.9454	-1.2582	$v_5$	4.7887	4.7612	2.7502

n1	0.9965	n6	0.9909	n11	1.0000	n16	1.0019	n21	0.9999	n26	1.0041	n31	0.9980
n2	1.0066	n7	0.9983	n12	1.0036	n17	1.0013	n22	0.9900	n27	1.0100	$\tilde{n}1$	0.9989
n3	1.0028	n8	0.9937	n13	1.0039	n18	1.0026	n23	1.0033	n28	1.0100	$\tilde{n}2$	1.0056
n4	1.0011	n9	1.0080	n14	1.0057	n19	1.0014	n24	1.0075	n29	0.9992		
n5	1.0037	n10	1.0000	n15	1.0065	n20	1.0053	n25	1.0088	n30	1.0069		

Table A.2: The parameters obtained from the fit to the combined PRad and MAMI data based on dispersion relations: Vector meson (upper panel) and normalization (lower panel) parameters. The normalization constants  $n1, \dots, n31$  refer to the MAMI data sets, whereas  $\tilde{n}1, \tilde{n}2$  normalize the PRad data. Masses  $m_V$  are given in GeV and couplings  $a_i^V$  in  $\text{GeV}^2$ .

Some remarks on the results presented in this table are in order. As in earlier dispersion-theoretical analyses, see e.g. [6, 7, 19], we find no OZI suppression for the couplings of the  $\phi$ . However, there is some close-by pole (here,  $v_1$ ) which cancels a large part of the  $\phi$  contribution (as noted in the main text, one cannot perform an isospin separation fitting only proton data). This will certainly change once neutron data are included, see e.g. [19]. For that reason, we also did not consider the uncertainties of the  $\bar{K}K$  and  $\pi\rho$  continua, as there are a) sizeable cancellations in this mass region and b) this region is of minor importance for the radius extraction. We also note that the tensor coupling of the  $\omega$  is expected to be suppressed in vector meson dominance due to the smallness of the isoscalar nucleon anomalous magnetic moment. This we indeed confirm consistently with the earlier works [6, 7, 19, 22, 20].

## References

- [1] C. E. Carlson, Prog. Part. Nucl. Phys. **82**, 59 (2015) [arXiv:1502.05314 [hep-ph]].
- [2] H.-W. Hammer and U.-G. Meißner, Sci. Bull. **65**, 257 (2020) [arXiv:1912.03881 [hep-ph]].
- [3] J. P. Karr, D. Marchand and E. Voutier, Nature Rev. Phys. **2**, 601 (2020).
- [4] G. F. Chew, R. Karplus, S. Gasiorowicz and F. Zachariasen, Phys. Rev. **110**, 265 (1958).
- [5] P. Federbush, M. L. Goldberger and S. B. Treiman, Phys. Rev. **112**, 642 (1958).
- [6] G. Höhler, E. Pietarinen, I. Sabba Stefanescu, F. Borkowski, G. G. Simon, V. H. Walther and R. D. Wendling, Nucl. Phys. B **114**, 505 (1976).
- [7] P. Mergell, U.-G. Meißner and D. Drechsel, Nucl. Phys. A **596**, 367 (1996) [arXiv:hep-ph/9506375 [hep-ph]].

- [8] G. P. Lepage and S. J. Brodsky, *Phys. Rev. D* **22**, 2157 (1980).
- [9] W. R. Frazer and J. R. Fulco, *Phys. Rev. Lett.* **2**, 365 (1959).
- [10] G. Höhler and E. Pietarinen, *Phys. Lett. B* **53**, 471 (1975).
- [11] M. Hoferichter, J. Ruiz de Elvira, B. Kubis and U.-G. Meißner, *Phys. Rept.* **625**, 1 (2016) [arXiv:1510.06039 [hep-ph]].
- [12] M. Hoferichter, B. Kubis, J. Ruiz de Elvira, H. W. Hammer and U.-G. Meißner, *Eur. Phys. J. A* **52**, 331 (2016) [arXiv:1609.06722 [hep-ph]].
- [13] D. Djukanovic, T. Harris, G. von Hippel, P. M. Junnarkar, H. B. Meyer, D. Mohler, K. Ottnad, T. Schulz, J. Wilhelm and H. Wittig, [arXiv:2102.07460 [hep-lat]].
- [14] W. Xiong, A. Gasparian, H. Gao, D. Dutta, M. Khandaker, N. Liyanage, E. Pasyuk, C. Peng, X. Bai and L. Ye, *et al. Nature* **575**, 147 (2019).
- [15] J. C. Bernauer *et al.* [A1], *Phys. Rev. C* **90**, 015206 (2014) [arXiv:1307.6227 [nucl-ex]].
- [16] J. M. Alarcón, D. W. Higinbotham and C. Weiss, *Phys. Rev. C* **102**, 035203 (2020) [arXiv:2002.05167 [hep-ph]].
- [17] Z. F. Cui, D. Binosi, C. D. Roberts and S. M. Schmidt, [arXiv:2102.01180 [hep-ph]].
- [18] H. Atac, M. Constantinou, Z.-E. Meziani, M. Paolone and N. Sparveris, *Eur. Phys. J. A* **57**, 65 (2021).
- [19] M. A. Belushkin, H.-W. Hammer and U.-G. Meißner, *Phys. Rev. C* **75**, 035202 (2007) [arXiv:hep-ph/0608337 [hep-ph]].
- [20] I. T. Lorenz, U.-G. Meißner, H.-W. Hammer and Y. B. Dong, *Phys. Rev. D* **91**, 014023 (2015) [arXiv:1411.1704 [hep-ph]].
- [21] I. Sabba Stefanescu, *J. Math. Phys.* **21**, 175 (1980).
- [22] I. T. Lorenz, H.-W. Hammer and U.-G. Meißner, *Eur. Phys. J. A* **48**, 151 (2012) [arXiv:1205.6628 [hep-ph]].
- [23] G. Paz, [arXiv:2004.03077 [hep-ph]].
- [24] S. Leupold, *Eur. Phys. J. A* **54**, 1 (2018) [arXiv:1707.09210 [hep-ph]].
- [25] <https://physics.nist.gov/cgi-bin/cuu/Value?rp>
- [26] A. A. Filin, V. Baru, E. Epelbaum, H. Krebs, D. Möller and P. Reinert, *Phys. Rev. Lett.* **124**, 082501 (2020). [arXiv:1911.04877 [nucl-th]].
- [27] C. Alexandrou, K. Hadjiyiannakou, G. Koutsou, K. Ottnad and M. Petschlies, *Phys. Rev. D* **101** (2020), 114504 [arXiv:2002.06984 [hep-lat]].
- [28] G. Ron *et al.* [Jefferson Lab Hall A], *Phys. Rev. C* **84**, 055204 (2011) [arXiv:1103.5784 [nucl-ex]].
- [29] X. Zhan, K. Allada, D. S. Armstrong, J. Arrington, W. Bertozzi, W. Boeglin, J. P. Chen, K. Chirapatpimol, S. Choi and E. Chudakov, *et al. Phys. Lett. B* **705**, 59 (2011) [arXiv:1102.0318 [nucl-ex]].